Vertical variations of flux parameters in irradiation channels at the TRIGA Mark II reactor of Pavia

Vertical variations of flux parameters in irradiation channels at the TRIGA Mark II reactor of Pavia

M. Di Luzio[a,*], G. D'Agostino[a], M. Oddone[b,a], A. Salvini[c]

[a] *Istituto Nazionale di Ricerca Metrologica (INRIM) - Unit of radiochemistry and spectroscopy, c/o Department of Chemistry, University of Pavia, Viale Taramelli 12; 27100 Pavia, Italy*
[b] *Department of Chemistry - Radiochemistry area, University of Pavia, Viale Taramelli 12; 27100 Pavia, Italy*
[c] *Laboratorio di Energia Nucleare Applicata (LENA), Via Aselli 41; 27100 Pavia, Italy*

Abstract

The knowledge of neutron flux parameters, both in terms of value and gradient, in irradiation channels of nuclear reactors is required to avoid biased results when applying Neutron Activation Analysis. To this aim, the Au-Zr bare triple-monitor method with the addition of Lu as a temperature monitor was used to collect experimental data in irradiation channels of three facilities at the TRIGA Mark II reactor of Pavia. Twenty-four monitors were placed in as many positions to determine the vertical variations of the neutron flux parameters. The results obtained in three different activation experiments pointed out a decrease of the conventional fluxes up to 70% in some cases. Nevertheless, the epithermal neutron flux correction factor, the thermal to epithermal neutron flux ratio and the modified spectral index were constant throughout the entire length of the channels within the core whereas trends were identified in channels outside the core.

Keywords: Neutron flux, Neutron Activation Analysis, TRIGA Mark II reactor

*Corresponding author
Email address: m.diluzio@inrim.it (M. Di Luzio)

1. Introduction

The energy distribution of neutrons produced in research nuclear reactors are described by flux parameters depending on the adopted convention. The accurate knowledge of these parameters becomes of fundamental importance when performing Neutron Activation Analysis (NAA) to model the activation of target nuclides in samples.

A number of facilities consisting of one or more vertical channels are usually available for irradiation in a reactor. Although a single channel can accommodate several piled-up samples, flux parameters are not likely to remain constant in space. It was in fact observed, at the 2 MW Interfaculty Reactor Institute in Delft, a significant variation of the investigated flux parameters (several tens of percent with respect to the average value) within a regular, 9 cm length, irradiation container albeit the study highlighted the absence of a defined underlying pattern.[1] Large spread in flux intensity is also expected among channels. As a matter of fact, at the 250 kW TRIGA Mark II reactor of Ljubljana a difference in flux intensity of a factor 7 was estimated between the channel placed at the center of the core and the carousel facility situated outside the core. Moreover, also among the forty irradiation channels of carousel facility, fluctuations in the order of 20% were observed.[2]

Recently, the k_0-NAA standardization method was applied at the Radiochemistry and Spectroscopy Laboratory of the Istituto Nazionale di Ricerca Metrologica using the 250 kW TRIGA Mark II nuclear reactor operated by the University of Pavia.[3] The adopted values for the flux parameters were obtained in previous measurements carried out in single positions of different channels. The Cd covered method was used with a set of flux monitors containing Au, Co, Zr and Rb.[4]

In this framework, aiming at reaching the ultimate accuracy in the application of relative- and k_0-NAA, we investigated the vertical variation of neutron flux parameters in the irradiation facilities. Significant differences were expected due to the very large length of channels with respect to their diameters.

The bare triple-monitor method[5] with a set of flux monitors containing Au and Zr was adopted to obtain the best position resolution while avoiding the replication of the experiment with and without the Cd cover. In detail, we measured (i) the epithermal neutron flux correction factor, (ii) the thermal to epithermal neutron flux ratio, (iii) the modified spectral index, and (iv) the (conventional) thermal, epithermal and fast fluxes. Additionally, (v) the neutron temperature was measured with Lu monitor in a single point of each irradiation facility.

In the following, after recalling the measurement models used to estimate the flux parameters, we describe the experimental setups and report the results, including the normalized vertical gradients of the thermal and epithermal fluxes.

2. Measurement models

Flux monitors are nuclides converted by neutron capture reactions to radionuclides which are successively quantified through their emitted γ-rays. Estimates of flux parameters are obtained from the knowledge of the amounts and nuclear parameters of the selected monitors and the outcome of γ-spectrometry measurements.

Theory and practical aspects regarding the techniques developed to determine flux parameters are described in details in literature.[6] Here we recall the measurement models adopted in this study starting from the basic equations.

The activation of a nuclide detected with γ-spectrometry is modeled by the following formula:

$$\frac{A_{\mathrm{sp}} M}{\theta \Gamma \varepsilon k_{\mathrm{sa}} R} = N_{\mathrm{A}}, \tag{1}$$

where A_{sp} is the specific γ-count rate at saturation, M is the molar mass of the target element, θ is the isotopic abundance of target isotope, Γ is the number of emitted gamma rays per disintegration, ε is the full-energy peak detection efficiency, k_{sa} is the gamma self-absorption correction factor, R is the production rate per target nucleus, and N_{A} is the Avogadro constant.

Specifically, in case the target nuclide follows a direct activation-decay path,

$$A_{\mathrm{sp}} = \frac{(n_{\mathrm{p}}\lambda t_{\mathrm{c}})}{t_{\mathrm{l}}(1-e^{-\lambda t_{\mathrm{i}}})e^{-\lambda t_{\mathrm{d}}}(1-e^{-\lambda t_{\mathrm{c}}})COIw}, \tag{2}$$

where n_{p} is the net area of the full-energy γ-peak, λ is the decay constant of the activated nuclide, t_{i} is the irradiation time, t_{d} is the time interval between the end of irradiation and the start of acquisition of γ-spectrum, t_{c} and t_{l} are the real and live times of the acquired γ-spectrum, COI is the true-coincidence correction factor for gammas emitted in cascade and w is the mass of the target element.

In the case of complex activation-decays, different formulae are available to calculate A_{sp}. For example, when the analytically interesting radionuclide is the daughter, II, of the directly formed one, I, the following equation applies:

$$A_{\mathrm{sp}} = \frac{n_{\mathrm{p,II}}t_{\mathrm{c}}}{t_{\mathrm{l}}w}\frac{\lambda_{\mathrm{II}}-\lambda_{\mathrm{I}}}{\lambda_{\mathrm{II}}\lambda_{\mathrm{I}}^{-1}S_{\mathrm{I}}D_{\mathrm{I}}C_{\mathrm{I}}-\lambda_{\mathrm{I}}\lambda_{\mathrm{II}}^{-1}S_{\mathrm{II}}D_{\mathrm{II}}C_{\mathrm{II}}}, \tag{3}$$

where S, D and C are $1-e^{-\lambda t_{\mathrm{i}}}$, $e^{-\lambda t_{\mathrm{d}}}$ and $1-e^{-\lambda t_{\mathrm{c}}}$, respectively, and subscripts I and II refer to the produced radionuclides.

In addition, $R = G_{\mathrm{s}}\Phi_{\mathrm{th}}\sigma_0 + G_{\mathrm{e}}\Phi_{\mathrm{e}}I_0(\alpha)$ if the Hogdahl convention is adopted for nuclides with $1/v$ neutron capture cross section[6], or $R = nv_0\sigma_0(G_{\mathrm{th}}g(T_{\mathrm{n}}) + G_{\mathrm{r}}r(\alpha)\sqrt{\frac{T_{\mathrm{n}}}{T_0}}s_0(\alpha))$ when the modified Westcott formalism is exploited instead for nuclides that do not follow the $1/v$ behavior[7]. Among the parameters in R definitions, G_{s} is the (Hogdahl) thermal (sub-cadmium) neutron self-shielding factor, Φ_{th} is the conventional thermal neutron flux, σ_0 is the (n,γ) reaction cross section at $2200\,\mathrm{m\,s^{-1}}$ neutron velocity, v_0, G_{e} is the (Hogdahl) epithermal (epi-cadmium) neutron self-shielding factor, Φ_{e} is the conventional epithermal neutron flux, α is the epithermal neutron flux correction factor, $I_0(\alpha)$ is the resonance integral for a $1/E^{1+\alpha}$ epithermal flux, n is the total neutron density, G_{th} is the (Westcott) thermal neutron self-shielding factor, $g(T_{\mathrm{n}})$ is the Westcott factor at the neutron temperature T_{n}, G_{r} is the resonance neutron self-shielding, $r(\alpha)\sqrt{\frac{T_{\mathrm{n}}}{T_0}}$ is the modified spectral index, which includes the epithermal to total

neutron density ratio, and $s_0(\alpha)$ is the resonance to thermal (n,γ) cross section ratio.

2.1. Bare triple-monitor method

The bare triple-monitor method is based on the use of three monitors. The combination of Eq.(1) multiplied by $\frac{\theta_{\mathrm{Au}}\Gamma_{\mathrm{Au}}\sigma_{\mathrm{Au}}}{M_{\mathrm{Au}}}$ and applied to monitors 1 and 2 provides the following formula:

$$\frac{A_{\mathrm{sp},1}\sigma_{0,1}}{k_{0,\mathrm{Au}}(1)\varepsilon_1 k_{\mathrm{sa},1}R_1} = \frac{A_{\mathrm{sp},2}\sigma_{0,2}}{k_{0,\mathrm{Au}}(2)\varepsilon_2 k_{\mathrm{sa},2}R_2}, \tag{4}$$

where subscripts 1 and 2 refer to the two monitors and $k_{0,\mathrm{Au}}(i) = \frac{\theta_i\Gamma_i\sigma_i M_{\mathrm{Au}}}{\theta_{\mathrm{Au}}\Gamma_{\mathrm{Au}}\sigma_{\mathrm{Au}}M_i}$ is a composite nuclear standardization factor referred to an element i with respect to the Au standard.[6]

In the case of Hogdahl convention and under the assumption that $\Phi_{\mathrm{th},1} = \Phi_{\mathrm{th},2}$ and $\Phi_{\mathrm{e},1} = \Phi_{\mathrm{e},2}$, i.e. the monitors are exposed to the same flux, Eq.(4) can be rearranged to obtain the conventional thermal to epithermal flux ratio:

$$f = \frac{\frac{k_{0,\mathrm{Au}}(1)\varepsilon_1}{k_{0,\mathrm{Au}}(2)\varepsilon_2}G_{\mathrm{e},1}Q_{0,1}(\alpha) - \frac{A_{\mathrm{sp},1}k_{\mathrm{sa},2}}{A_{\mathrm{sp},2}k_{\mathrm{sa},1}}G_{\mathrm{e},2}Q_{0,2}(\alpha)}{G_{\mathrm{s}}\left(\frac{A_{\mathrm{sp},1}k_{\mathrm{sa},2}}{A_{\mathrm{sp},2}k_{\mathrm{sa},1}} - \frac{k_{0,\mathrm{Au}}(1)\varepsilon_1}{k_{0,\mathrm{Au}}(2)\varepsilon_2}\right)}, \tag{5}$$

where $Q_0(\alpha) = \frac{I_0(\alpha)}{\sigma_0} = \frac{Q_0 - 0.429}{\bar{E}_{\mathrm{r}}^{\alpha}} + \frac{0.429}{(2\alpha+1)0.55^{\alpha}}$; Q_0 is the resonance integral to σ_0 for a $1/E$ epithermal flux and $\bar{E}_{\mathrm{r}}$ is the effective resonance energy that is considered independent from α.[8]

In the case of Westcott convention and under the assumption that the monitors are exposed to the same thermal and epithermal neutron densities, from Eq.(4) it derives the so called modified spectral index:

$$r(\alpha)\sqrt{\frac{T_{\mathrm{n}}}{T_0}} = \frac{G_{\mathrm{th}}\left(\frac{A_{\mathrm{sp},1}k_{\mathrm{sa},2}}{A_{\mathrm{sp},2}k_{\mathrm{sa},1}}g_2(T_{\mathrm{n}}) - \frac{k_{0,\mathrm{Au}}(1)\varepsilon_1}{k_{0,\mathrm{Au}}(2)\varepsilon_2}g_1(T_{\mathrm{n}})\right)}{\frac{k_{0,\mathrm{Au}}(1)\varepsilon_1}{k_{0,\mathrm{Au}}(2)\varepsilon_2}G_{\mathrm{r},1}s_{0,1}(\alpha) - \frac{A_{\mathrm{sp},1}k_{\mathrm{sa},2}}{A_{\mathrm{sp},2}k_{\mathrm{sa},1}}G_{\mathrm{r},2}s_{0,2}(\alpha)}, \tag{6}$$

It is worth to note that the knowledge of α is required to compute f and $r(\alpha)\sqrt{\frac{T_{\mathrm{n}}}{T_0}}$. The use of three $1/v$ monitors is suitable to estimate α by com-

bining Eq.(5) applied to monitors 1 and 2 and to monitors 1 and 3, rearranged to obtain the following equation:

$$\left(\frac{1}{\frac{A_{\mathrm{sp},1}k_{\mathrm{sa},2}k_{0,\mathrm{Au}}(2)\varepsilon_2}{A_{\mathrm{sp},2}k_{\mathrm{sa},1}k_{0,\mathrm{Au}}(1)\varepsilon_1}-1}-\frac{1}{\frac{A_{\mathrm{sp},1}k_{\mathrm{sa},3}k_{0,\mathrm{Au}}(3)\varepsilon_3}{A_{\mathrm{sp},3}k_{\mathrm{sa},1}k_{0,\mathrm{Au}}(1)\varepsilon_1}-1}\right)$$
$$\times G_{\mathrm{e},1}Q_{0,1}(\alpha)-\left(\frac{1}{1-\frac{A_{\mathrm{sp},2}k_{\mathrm{sa},1}k_{0,\mathrm{Au}}(1)\varepsilon_1}{A_{\mathrm{sp},1}k_{\mathrm{sa},2}k_{0,\mathrm{Au}}(2)\varepsilon_2}}\right)G_{\mathrm{e},2}Q_{0,2}(\alpha) \tag{7}$$
$$+\left(\frac{1}{1-\frac{A_{\mathrm{sp},3}k_{\mathrm{sa},1}k_{0,\mathrm{Au}}(1)\varepsilon_1}{A_{\mathrm{sp},1}k_{\mathrm{sa},3}k_{0,\mathrm{Au}}(3)\varepsilon_3}}\right)G_{\mathrm{e},3}Q_{0,3}(\alpha)=0,$$

where subscripts 1, 2, 3 refer to the three monitors. The α value is obtained numerically as the implicit solution of Eq.(7).

There is a combination of monitors providing the practically attainable lowest uncertainty for the determination of α. Specifically, the three monitors should have the largest possible spread in the $\bar{E}_{\mathrm{r}}$ and Q_0 values.[5] Among the different monitor data sets developed and tested, the most used consists of ^{197}Au, ^{94}Zr and ^{96}Zr and the adopted neutron capture reactions are ^{197}Au(n,γ)^{198}Au, ^{94}Zr(n,γ)^{95}Zr and ^{96}Zr(n,γ,$\beta-$)$^{97\mathrm{m}}$Nb. This combination gives practical advantages because Zr provides two monitors reflecting in a simpler sample preparation; in addition, as the adopted gammas are not emitted in cascade, they are not affected by true-coincidences ($COI = 1$).

2.2. Conventional thermal, epithermal and fission neutron fluxes

The conventional thermal and epithermal neutron fluxes are computed from the following equations applied to one of the three monitors and obtained by rearranging Eq.(1):

$$\Phi_{\mathrm{th}}=\frac{A_{\mathrm{sp}}M}{\theta\Gamma\varepsilon k_{\mathrm{sa}}N_{\mathrm{A}}\sigma_0\left(G_{\mathrm{s}}+G_{\mathrm{e}}\frac{Q_0(\alpha)}{f}\right)}, \tag{8}$$

$$\Phi_{\mathrm{e}}=\frac{A_{\mathrm{sp}}M}{\theta\Gamma\varepsilon k_{\mathrm{sa}}N_{\mathrm{A}}\sigma_0\left(G_{\mathrm{s}}f+G_{\mathrm{e}}Q_0(\alpha)\right)}. \tag{9}$$

The fission component can be retrieved using monitor sets containing a nuclide activated through fast neutrons. Among the available nuclides, a convenient choice is the ^{90}Zr via the reaction ^{90}Zr(n,2n)^{89}Zr. In this case the reaction rate per target nucleus is due to the fission component, i.e. $R = \Phi_{\rm f}\sigma_{\rm f}$, where $\Phi_{\rm f}$ is the conventional fission flux and $\sigma_{\rm f}$ is the ^{235}U spectrum averaged cross section for the reaction ^{90}Zr(n,2n)^{89}Zr.[6] From Eq.(1) it follows:

$$\Phi_{\rm f} = \frac{A_{\rm sp} M}{\theta \Gamma \varepsilon k_{\rm sa} N_{\rm A} \sigma_{\rm f}}. \tag{10}$$

2.3. Neutron temperature

A further monitor added to the bare triple-monitor allows the measurement of the neutron temperature. For this purpose, Lu is generally adopted via the reaction ^{176}Lu(n,γ)^{177}Lu. Since the isotope ^{176}Lu is a non $1/v$ nuclide, $g_{\rm Lu}(T_{\rm n})$ deviates from unity according to $T_{\rm n}$.[9]

The $g_{\rm Lu}(T_{\rm n})$ value is obtained from Eq.(6) applied to Lu and one of the available $1/v$ monitors, say monitor 1. Accordingly,

$$\begin{aligned} g_{\rm Lu}(T_{\rm n}) = \frac{1}{G_{\rm th,Lu}} \Bigg(& \frac{A_{\rm sp,Lu} k_{0,\rm Au}(1) \varepsilon_1 k_{\rm sa,1}}{A_{\rm sp,1} k_{0,\rm Au}({\rm Lu}) \varepsilon_{\rm Lu} k_{\rm sa,Lu}} \\ & \times \left(G_{\rm th,1} g_1(T_{\rm n}) + G_{\rm r,1} r(\alpha) \sqrt{\frac{T_{\rm n}}{T_0}} s_{0,1}(\alpha) \right) \\ & - G_{\rm r,Lu} r(\alpha) \sqrt{\frac{T_{\rm n}}{T_0}} s_{0,\rm Lu}(\alpha) \Bigg), \end{aligned} \tag{11}$$

where subscripts Lu and 1 refer to Lu and the monitor used as comparator, respectively. It is worth noting that as monitor 1 follows $1/v$ behavior, $g_1(T_{\rm n}) \cong 1$. The $s_0(\alpha)$ value can be obtained from $s_0(\alpha) = \frac{s_0}{E_{\rm r}^{\alpha}}$,[10] where s_0 is available in literature for non $1/v$ monitors while it can be computed from $s_0 = \frac{2}{\sqrt{\pi}}(Q_0 - 0.429)$ for $1/v$ monitors. The $T_{\rm n}$ value is finally estimated from the measured $g_{\rm Lu}(T_{\rm n})$ using the (known) function linking $g_{\rm Lu}(T_{\rm n})$ to $T_{\rm n}$.[11]

3. Experimental

3.1. Irradiation facilities

The TRIGA Mark II working in Pavia is a 250 kW pool-type research reactor fueled with low-enriched ^{235}U and moderated with demineralized light water. At present, the reactor operates weekly from Monday to Friday for about 30 h non-continuously.

The core is composed by ninety slots occupied by fuel elements, neutron sources and three control rods (SHIM, REG and TRANS) placed in five concentric rings around a central channel, 40 cm useful length and 26 mm diameter, used as irradiation facility and called Central Channel, CC. One of the slots of the outer ring houses a channel, 10 cm useful length and 15 mm diameter, used as a short time irradiation facility and called Rabbit, RB. Additional forty channels, 27 cm useful length and 26 mm diameter, coded from 1 to 40 and located in a carousel inside a graphite reflector surrounding the core, are available in an irradiation facility called Lazy Susan, LS. Samples are manually inserted in the irradiation channels with the exception of the Rabbit facility, where a pneumatic system is available for users.[12] The position of the irradiation facilities is shown in the schematic horizontal cross section of the reactor displayed in Fig.1.

3.2. Preparation and neutron exposure of monitor samples

In this study we measured the neutron flux parameters using 24 monitor samples distributed in as many irradiation positions. Specifically, 10 samples were located in CC, 5 in RB, 3 in LS-26, and 6 in LS-27.

Each monitor sample was prepared by weighing 30 µL volume of a mono-elemental Au solution pipetted on a 6 mm diameter filter paper disk placed in a 1 mL polyethylene (PE) vial. In a few cases, 30 µL volume of a mono-elemental Lu solution was added to probe the neutron temperature. After drying with an infrared lamp, a 6 mm diameter disk of pure Zr was pressed on the filter paper disk. The vial was finally heat-sealed to avoid vertical displacements. A sketch of the monitor sample in its 1 mL vial is zoomed in Fig.2.

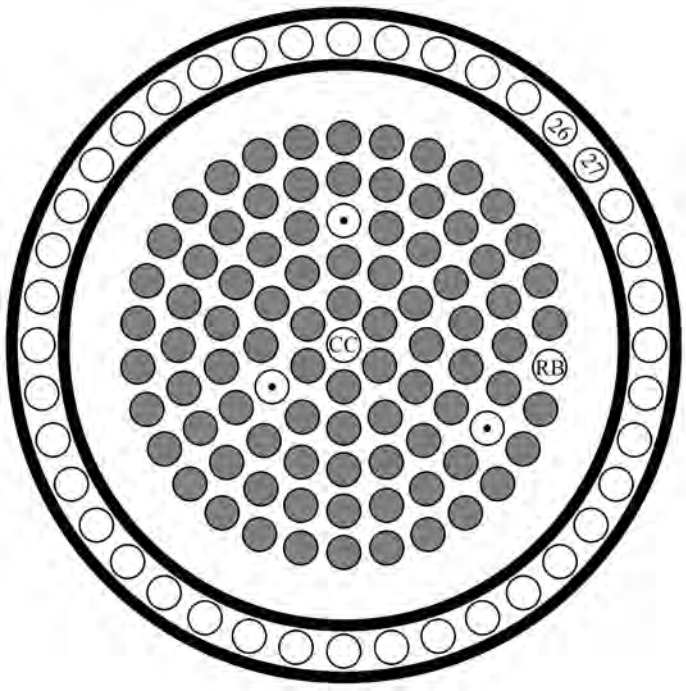

Figure 1: Schematic horizontal cross section of the TRIGA Mark II reactor of Pavia. The inner small circles represents the slots of the reactor core, including the Central Channel, CC, and Rabbit, RB, facilities and three control rods (SHIM, TRANS and REG situated in the second, third and fourth concentric ring from CC, respectively) marked with a dot. The two external rings represent the graphite reflectors surrounding the core and housing the forty channels (small circles) of the Lazy Susan facility, LS; the position of channels LS-26 and LS-27 is indicated.

Specifically, two solutions, S_{Au1} and S_{Au2}, were prepared by dilution 1:15 and 1:6 of a SI traceable 1000 µg mL^{-1} Au standard solution, Sigma-Aldrich. S_{Au1} was used for monitors in CC and RB, S_{Au2} was used for monitors in LS. In the case of monitor samples including Lu, an SI traceable 1000 µg mL^{-1} Lu standard solution, Sigma-Aldrich, was used. Disks of Zr, 99.2% purity, 0.1 mm and 0.5 mm thickness, GoodFellow, were used; the thin ones in CC and RB, and the thick ones in LS.

The masses of the pipetted solutions and disks were measured using a SI traceable analytical balance.

It is worth to note that total thickness of the stacked filter paper and Zr disk was kept lower than 1 mm. This assured a good spatial resolution of the measurement and a negligible vertical variation of the probed neutron flux.

The vials were fixed in equally spaced vertical positions at the center axis of PE irradiation containers using PE inserts. The monitor samples used in CC, RB and LS were distributed in 3, 1 and 3 containers, respectively, and sent to irradiation. The layouts of monitors in the containers placed in the different facilities are shown in Fig.2. The vertical distance, d, of each monitor with respect to the bottom of the piled-up containers is indicated.

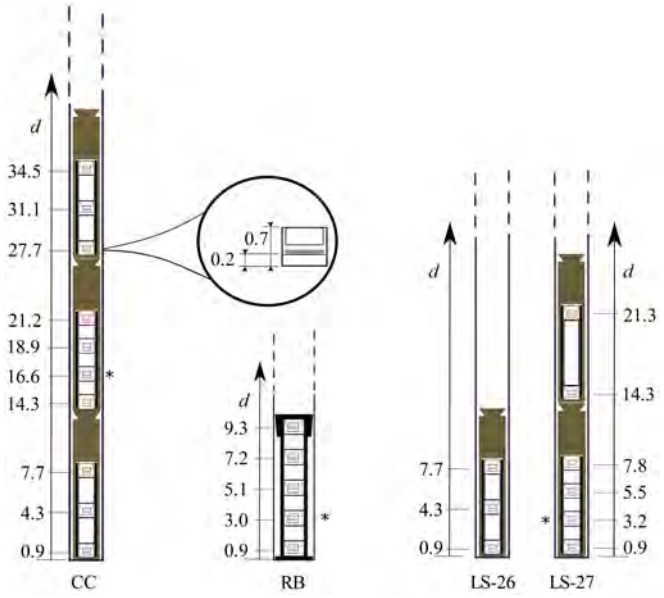

Figure 2: Layouts of the containers placed in the channels of the different irradiation facilities. The vertical position, d, of each monitor sample with respect to the bottom of the channel is showed. The asterisks indicate the monitors including Lu for neutron temperature measurements. The height of the 1 mL vial and the position of the monitor sample are shown in the zoom. Distances are in cm.

Three irradiations lasting 3600 s were sequentially performed with the reactor at 250 kW critical power. The first one was carried out in CC by introducing the containers with the reactor powered-off, whereas the second and the third

ones in RB and LS with the reactor powered-on. The carousel of LS facility was not rotating during the irradiation.

During irradiation, the TRANS control rod was completely extracted and the SHIM was fixed in a vertical position selected to maintain the critical power with the REG moving close to the equator of the core.

Sinusoidal displacements of REG around the central position were negligible. In addition, the vertical position of the REG was similar in the three irradiations. This is the typical layout of the control rods adopted when samples are irradiated for NAA to limit the variability of neutron flux parameters due to different arrangements of the control rods.[13]

3.3. Gamma spectrometry measurements

The 1 mL vials holding the monitors were extracted from the irradiation containers after about 16 h cooling time and fixed at the center of plastic circular containers for γ-counting. The γ-spectrometry measurements were carried out using a CANBERRA GC3518 HPGe detector (35% relative efficiency, 1.96 keV FWHM at 1332.5 keV energy) connected to an ORTEC DSPEC 502 multi-channel analyzer. Samples were manually placed at 10 cm distance from the end-cap of the GC3518 by means of a plastic spacer; this quite large distance was chosen to limit the effect of sample positioning. The detection system was calibrated in energy and efficiency using a certified multi-γ source.

Each monitor sample was counted twice. A first (short) acquisition, lasting about 1 h, was performed within 24 h after the irradiation end to quantify the 411.8 keV ^{198}Au, the 743.4 keV ^{97m}Nb and, if present, the 208.4 keV ^{177}Lu γ-peaks. After 2 or 3 days, a second (long) acquisition, lasting about 24 h, was performed to quantify the 756.7 keV ^{95}Zr and 909.2 keV ^{89}Zr γ-peaks. Acquisition times were online adjusted to determine the net area of the γ-peaks with a relative uncertainty due to counting statistics lower than 0.2%. During data collection, the pile-up rejection circuit was active and the recorded relative dead time was always below 10%.

4. Results and discussion

The forty-eight collected γ-spectra were processed using the moderate count rate and regular peaks algorithm of the HyperLab software to calculate the net area of the γ-peaks. The corresponding specific γ-count rates at saturation of ^{198}Au, ^{95}Zr, ^{89}Zr and ^{177}Lu were computed via Eq.(2) whereas Eq.(3) was used for ^{97m}Nb.

First, α was obtained by solving Eq.(7) with ^{197}Au, ^{94}Zr and ^{96}Zr as monitor 1, 2 and 3, respectively. The resulting α value was used to compute f and $r(\alpha)\sqrt{\frac{T_n}{T_0}}$ according to Eq.(5) and (6), respectively. The corresponding (Hogdahl) conventional fluxes Φ_{th}, Φ_e and Φ_f were calculated via Eq.(8), (9) and (10), respectively, using the ^{197}Au monitor. The ^{197}Au was also adopted as monitor 1 in Eq.(11) for the measurement of the neutron temperature.

The k_0, σ_0, Q_0, s_0, $\bar{E}_r$ and λ values, including their uncertainty, were retrieved from the k_0 database[14] while for σ_f the most up to date literature value was adopted.[15] The $Q_{0,Au}$ value was converted to $s_{0,Au}$ in order to apply Westcott formalism in Eq.(11). The M_{Au}, θ_{Au}, Γ_{Au} and N_A values adopted in Eq.(8), (9) and (10) were retrieved from literature.[16, 17, 18]

The effect of γ-rays self-absorption was neglected for Au and Lu pipetted on the filter paper while it was evaluated for Zr disks by taking into account thickness and linear attenuation coefficient at given γ-energies.[19] The resulting influence was negligible with the exception of the 0.5 mm thickness for which the k_{sa} correction factor was close to 0.99.

Thermal, sub-cadmium, epithermal and resonance self-shielding factors, G_{th}, G_s, G_e and G_r were assumed equal to unity with the exception of G_e for the ^{94}Zr and ^{96}Zr, calculated with the polynomial fit proposed by De Corte.[6]

The Westcott $g_{Au}(T_n)$ factor in Eq.(11) was also considered equal to the unity under the reasonable assumption that the Au cross section function follows a perfect $1/v$ behavior until 2 eV energy.

The above reported formulae were implemented in a Microsoft Excel spreadsheet to calculate α, f, $r(\alpha)\sqrt{\frac{T_n}{T_0}}$, Φ_{th}, Φ_e, Φ_f and T_n, including their combined

uncertainties evaluated by means of the sensitivity coefficient method. The main contributors to the evaluated uncertainties are shown in Table 1.

Parameter	1^{st} contributor	2^{nd} contributor	3^{rd} contributor
α / 1	ε	$k_{0,\mathrm{Au}}(^{94}\mathrm{Zr})$	$Q_{0,\mathrm{Au}}$
f / 1	α	$k_{0,\mathrm{Au}}(^{94}\mathrm{Zr})$	$Q_{0,^{96}\mathrm{Zr}}$
$r(\alpha)\sqrt{\frac{T_\mathrm{n}}{T_0}}$ / 1	α	$k_{0,\mathrm{Au}}(^{94}\mathrm{Zr})$	$s_{0,^{96}\mathrm{Zr}}$
Φ_th / $\mathrm{cm}^{-2}\,\mathrm{s}^{-1}$	f	ε	$Q_{0,\mathrm{Au}}$ / α
Φ_e / $\mathrm{cm}^{-2}\,\mathrm{s}^{-1}$	f	ε	$Q_{0,\mathrm{Au}}$ / α
Φ_f / $\mathrm{cm}^{-2}\,\mathrm{s}^{-1}$	σ_f	n_p	θ
$g_{\mathrm{Lu}}(T_\mathrm{n})$ / 1	$k_{0,\mathrm{Au}}(\mathrm{Lu})$	$r(\alpha)\sqrt{\frac{T_\mathrm{n}}{T_0}}$	$s_{0,\mathrm{Au}}$
T_n / °C	$g_{\mathrm{Lu}}(T_\mathrm{n})$	-	-

Table 1: Main contributors to the combined uncertainty for the measured flux parameters in CC, RB and LS ranked in descending order of importance.

The α and f values measured in CC, RB and LS-27 versus the distance d are plotted in Fig.3. In addition, the $r(\alpha)\sqrt{\frac{T_\mathrm{n}}{T_0}}$ values are shown in Fig.A.1 of the Appendix.

The measured α, f and $r(\alpha)\sqrt{\frac{T_\mathrm{n}}{T_0}}$ values in CC and RB did not show significant trends. Specifically, the α scattering was in agreement with the calculated α averages $-0.0347(91)$ and $-0.0356(92)$ in CC and RB, respectively. A similar agreement was observed for the f data with the averages 19.2(10) and 19.6(10) in CC and RB, respectively, and for the $r(\alpha)\sqrt{\frac{T_\mathrm{n}}{T_0}}$ data with the averages 0.0450(20) and 0.0442(20) in CC and RB, respectively. Here and hereafter, the uncertainties ($k = 1$) in parentheses apply to the last respective digits. The mean of the single evaluated uncertainties was assigned to the calculated average.

Significant linear trends were identified in LS-27; in addition, the agreement between the values recorded in LS-26 and LS-27 confirmed the trends and pointed out the absence of appreciable differences. The data obtained in LS-27 were fitted by a straight line $y = bd + c$ to quantify the slope, b, and the intercept, c, for α, f and $r(\alpha)\sqrt{\frac{T_\mathrm{n}}{T_0}}$. The b and c fitting parameters are reported in Table 2 together with the uncertainty, $u(y)$, of the value obtained when using the model y. The mean of the single evaluated uncertainties was assigned to

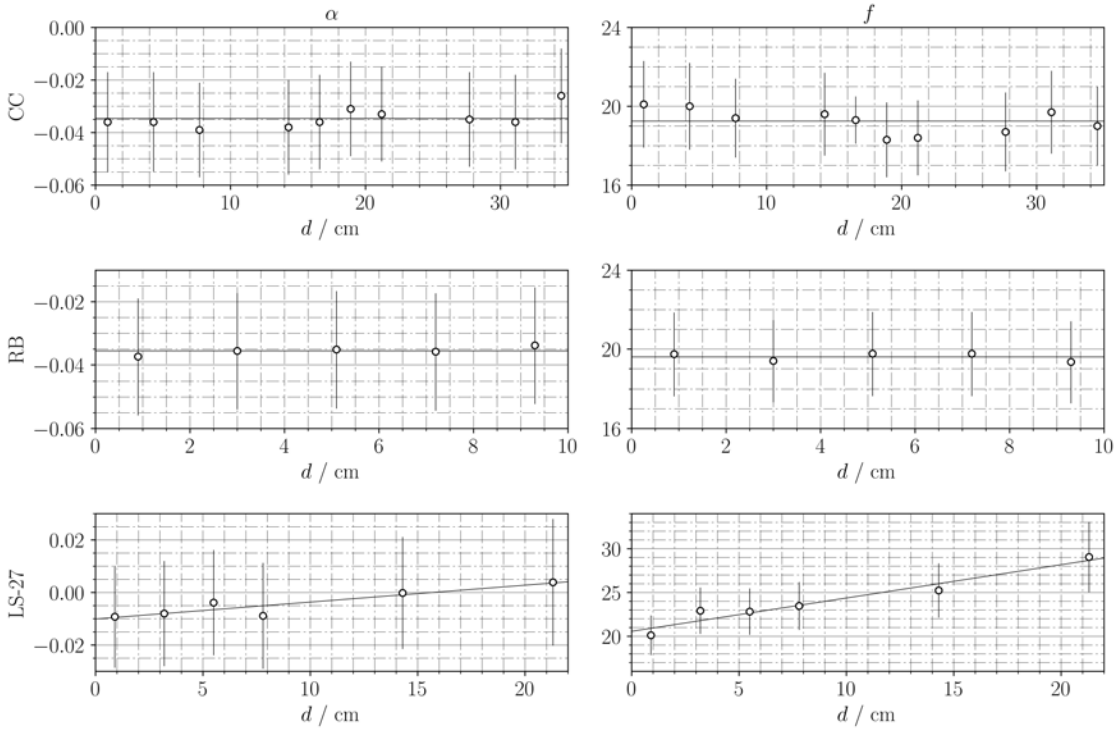

Figure 3: The α and f values measured in CC, RB and LS-27 at different vertical distance, d, with respect to the bottom of the stacked irradiation container. Error bars indicate the expanded ($k = 2$) uncertainties. Averages and straight lines fitting the data are displayed.

$u(y)$.

The Φ_{th} and Φ_{e} values measured in CC, RB and LS-27 versus the distance d are plotted in Fig.4. In addition, the Φ_{f} values are shown in Fig.A.1 of the Appendix.

Significant trends of the measured Φ_{th}, Φ_{e} and Φ_{f} values were identified in CC, RB and LS-27; the trends in LS-27 and the absence of appreciable differences with its adjacent channel were confirmed and pointed out by the results obtained with the 3 monitor samples located in LS-26. The data were fitted by a parabola $y = ad^2 + bd + c$ with the exception of the Φ_{e} and Φ_{f} values in LS-27 which were fitted by a straight line $y = bd + c$.

The a, b and c fitting parameters are reported in Table 3 together with the

Channel	Parameter / 1	b / cm^{-1}	c / 1	$u(y)$ / 1
LS-27	α	$6.4(14)\times10^{-4}$	-0.0101(16)	0.010
	f	0.380(48)	20.57(54)	1.5
	$r(\alpha)\sqrt{\frac{T_\mathrm{n}}{T_0}}$	$-5.40(86)\times10^{-4}$	0.04160(97)	0.0019

Table 2: Computed values for slope, b, and intercept, c, of the straight line $y = bd+c$ fitting the α, f and $r(\alpha)\sqrt{\frac{T_\mathrm{n}}{T_0}}$ values measured in LS-27. The fitting uncertainties ($k = 1$) in parentheses apply to the last respective digits. The uncertainty associated to y, $u(y)$, is given.

relative uncertainty, $u_\mathrm{r}(y)$, of the value obtained when using the model y. The mean of the single evaluated relative uncertainties was assigned to $u_\mathrm{r}(y)$.

Channel	Parameter / $\mathrm{cm}^{-2}\,\mathrm{s}^{-1}$	a / $\mathrm{cm}^{-4}\,\mathrm{s}^{-1}$	b / $\mathrm{cm}^{-3}\,\mathrm{s}^{-1}$	c / $\mathrm{cm}^{-2}\,\mathrm{s}^{-1}$	$u_\mathrm{r}(y)$ / 1
CC	Φ_th	$-1.111(40)\times10^{10}$	$3.35(15)\times10^{11}$	$4.17(11)\times10^{12}$	3.3%
	Φ_e	$-6.25(31)\times10^{8}$	$1.95(11)\times10^{10}$	$2.005(89)\times10^{11}$	3.7%
	Φ_f	$-8.11(89)\times10^{9}$	$2.48(33)\times10^{11}$	$2.58(25)\times10^{12}$	5.7%
RB	Φ_th	$-7.6(18)\times10^{9}$	$2.3(19)\times10^{10}$	$3.043(40)\times10^{12}$	3.4%
	Φ_e	$-3.35(34)\times10^{8}$	$7.7(35)\times10^{8}$	$1.5540(76)\times10^{11}$	3.7%
	Φ_f	$-1.02(50)\times10^{10}$	$8.5(53)\times10^{10}$	$1.37(11)\times10^{12}$	5.2%
LS-27	Φ_th	$-8.3(38)\times10^{8}$	$-8.5(88)\times10^{9}$	$1.219(36)\times10^{12}$	3.4%
	Φ_e	-	$-1.704(72)\times10^{9}$	$5.980(82)\times10^{10}$	3.9%
	Φ_f	-	$-5.53(27)\times10^{9}$	$2.053(30)\times10^{11}$	6.1%

Table 3: Computed values for a, b and c of the parabola $y = ad^2 + bd + c$ or the straight line $y = bd + c$ fitting the Φ_th, Φ_e and Φ_f data measured in CC, RB and LS-27. The fitting uncertainties ($k = 1$) in parentheses apply to the last respective digits. The relative uncertainty associated to y, $u_\mathrm{r}(y)$, is given.

A quantitative information on the effect of the local deviations can be pointed out by the normalized gradient of the conventional flux, $\upsilon(\Phi) = \frac{1}{\Phi}\frac{\partial\Phi}{\partial d}$. The results based on parabolas and straight lines fitting Φ_th and Φ_e in CC, RB and LS are plotted in Fig.5.

The $g_\mathrm{Lu}(T_\mathrm{n})$ values in CC, RB and LS-27 resulted to be 1.94(11), 1.84(11) and 1.85(11), respectively, corresponding to 54(16) °C, 35(15) °C and 40(15) °C neutron temperatures. Quoted uncertainties were due to the uncertainties of $g_\mathrm{Lu}(T_\mathrm{n})$ amplified by the function linking $g_\mathrm{Lu}(T_\mathrm{n})$ to T_n.

To sum up, the data pointed out that α was close to -0.035 both along the 40 cm length channel of CC and along the 10 cm length channel of RB whereas it showed a (small) positive trend across 0.00 along the 27 cm length channel

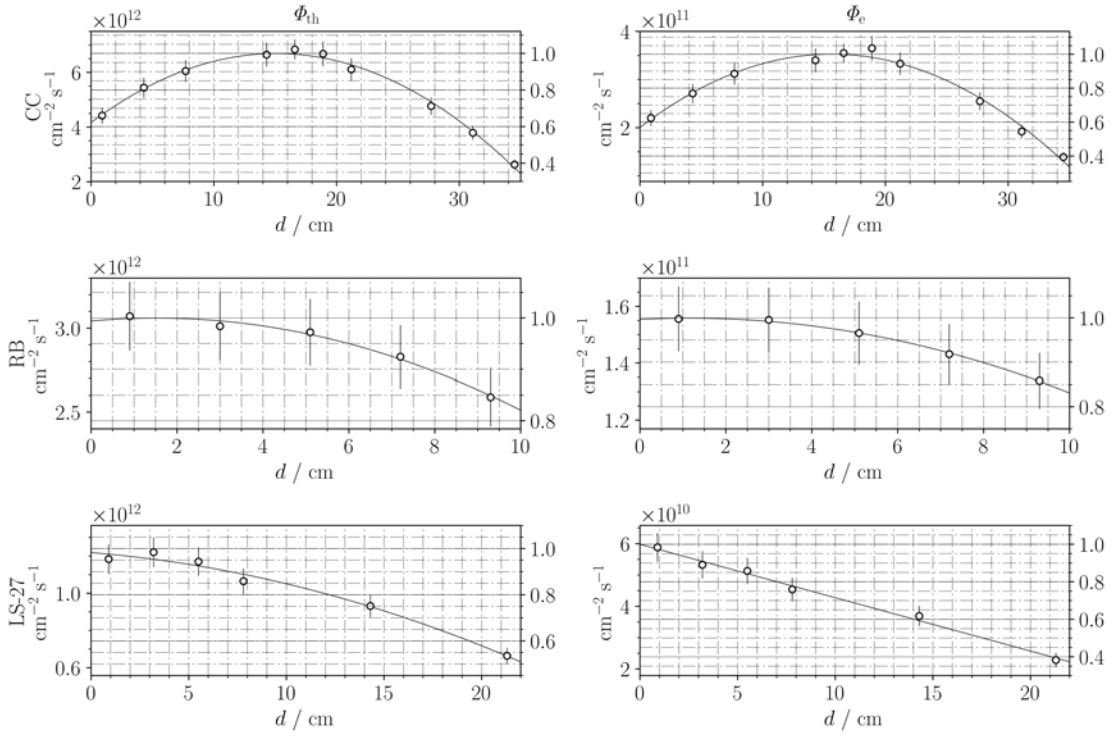

Figure 4: The Φ_{th} and Φ_{e} values measured in CC, RB and LS-27 at different vertical distance, d, with respect to the bottom of the stacked irradiation container. Error bars indicate the expanded ($k = 2$) uncertainties. Parabolas or straight lines fitting the data are displayed. The left side ordinate axis indicates the absolute value while the right side indicates the conventional flux normalized to the vertex of the parabola or to the intercept of the straight line.

of LS-27. Similarly, f was close to 20 both in CC and RB whereas it showed a (major) positive trend starting from 20 up to 30 in LS-27. In addition, $r(\alpha)\sqrt{\frac{T_{\mathrm{n}}}{T_0}}$ was close to 0.045 both in CC and RB whereas it showed a (major) negative trend starting from 0.040 up to 0.030 in LS-27.

Concerning the conventional fluxes, a noteworthy decrease of Φ_{th} and Φ_{e} up to 60% was observed in CC with respect to the $6.69(22) \times 10^{12}\,\mathrm{cm^{-2}\,s^{-1}}$ and $3.53(12) \times 10^{11}\,\mathrm{cm^{-2}\,s^{-1}}$ maximum, respectively, occurring at 15 cm distance from the bottom of the channel. A reduction of Φ_{f} up to 70% was detected with respect to the $4.47(27) \times 10^{12}\,\mathrm{cm^{-2}\,s^{-1}}$ maximum occurring at the same 15 cm

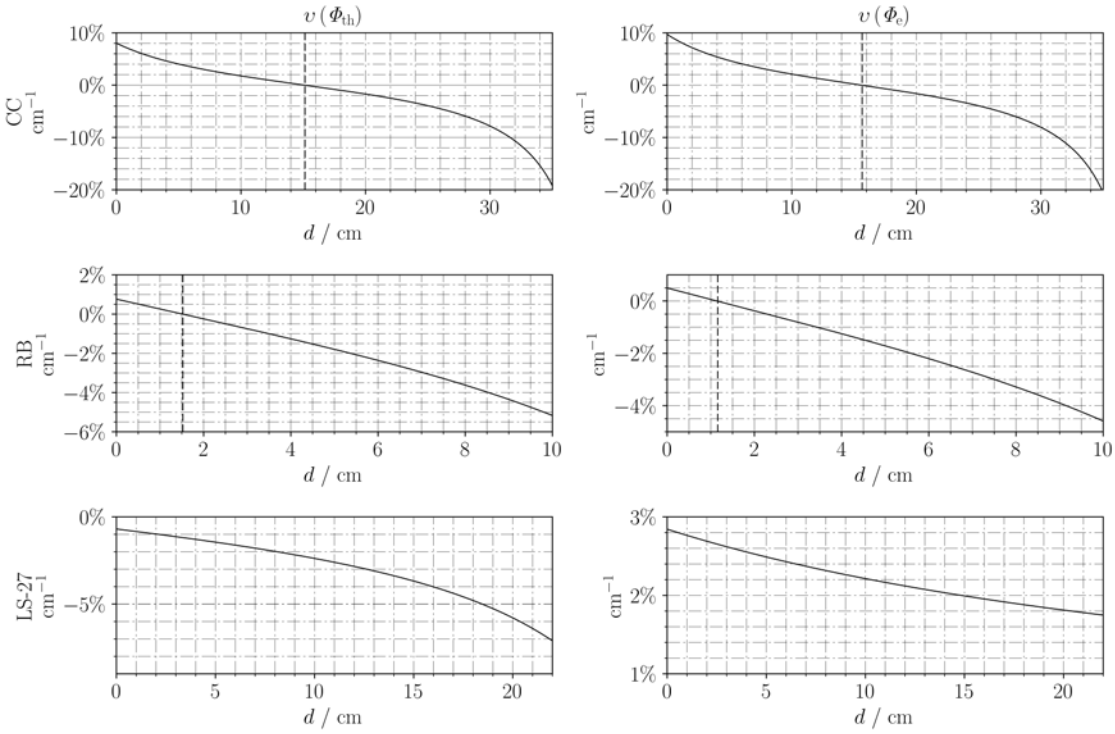

Figure 5: The normalized flux gradients, $\upsilon(\Phi_{th})$ and $\upsilon(\Phi_e)$, in CC, RB and LS-27 at different vertical distance, d, with respect to the bottom of the stacked irradiation container. Vertical dashed lines show the position where the first derivative of the flux is zero.

distance.

A minor but still significant decrease of Φ_{th} and Φ_e up to 20% was observed in RB with respect to the $3.06(10) \times 10^{12}\,cm^{-2}\,s^{-1}$ and $1.56(8) \times 10^{11}\,cm^{-2}\,s^{-1}$ maximum, respectively, occurring at 1.5 cm. A reduction of Φ_f up to 20% was detected with respect to the $1.55(8) \times 10^{12}\,cm^{-2}\,s^{-1}$ maximum occurring at 4 cm.

In LS-27, the results pointed out a remarkable decrease up to 50% of Φ_{th} and up to 60% of Φ_e with respect to the $1.24(4) \times 10^{12}\,cm^{-2}\,s^{-1}$ and $5.98(23) \times 10^{10}$ $cm^{-2}\,s^{-1}$ maximum, respectively, starting from the channel bottom. A reduction of Φ_f up to 60% was detected with respect to the $2.05(12) \times 10^{11}\,cm^{-2}\,s^{-1}$ maximum at the channel bottom.

The data collected in this study can be compared with the literature results reported in Table 4. Specifically, the α value measured in CC, RB and LS published in 2017[4] is in agreement, the f value is lower while the Φ_{th} and Φ_{e} values are within the variability range observed along the channels. Likewise, the f value measured in CC, RB and LS published in 2014[20] is lower whereas the Φ_{th} and Φ_{e} values are within and outside, respectively, the observed variability range.

	CC	RB	LS
[4]			
Φ_{th} / $\mathrm{cm}^{-2}\,\mathrm{s}^{-1}$	$6.11(16)\times10^{12}$	$2.54(7)\times10^{12}$	$1.02(3)\times10^{12}$
Φ_{e} / $\mathrm{cm}^{-2}\,\mathrm{s}^{-1}$	$3.92(6)\times10^{11}$	$1.62(3)\times10^{11}$	$5.88(9)\times10^{10}$
α / 1	-0.036(6)	-0.041(7)	-0.016(6)
f / 1	15.6(3)	15.7(4)	17.4(4)
[20](*)			
Φ_{th} / $\mathrm{cm}^{-2}\,\mathrm{s}^{-1}$	6.84×10^{12}	3.04×10^{12}	1.13×10^{12}
Φ_{e} / $\mathrm{cm}^{-2}\,\mathrm{s}^{-1}$	4.26×10^{11}	1.90×10^{11}	7.93×10^{10}
α / 1	-	-	-
f / 1	16.1	16.0	14.2

Table 4: Neutron flux parameters measured in previous experiments in CC, RB and LS. (*) Values obtained after conversion of the published integral flux data.

5. Conclusion

The knowledge of the variation of neutron flux parameters is a precondition to reach the ultimate accuracy when performing NAA in a reactor.

To this aim, vertical deviations of α, f, modified spectral index and conventional thermal, epithermal, fast fluxes were measured in the CC, RB and LS irradiation facilities of the TRIGA Mark II reactor of Pavia. Neutron temperature was also probed in single positions.

The reproducibility of the results allowed observing the profile of neutron flux parameters along the channels. Specifically, the conventional fluxes strongly decreased up to tens of percent in few centimeters when moving from the maximum in all the facilities. Nevertheless, no variations of f, modified spectral

index and α were detected in CC and RB while significant trends were identified in LS. In addition, the neutron temperature was higher in CC with respect to RB and LS.

Constant α and f values significantly simplify the NAA measurement equation only if the thermal and epithermal fluxes are constant too. The data collected in this study pointed out that the assumption of constant thermal and epithermal fluxes does not hold in a TRIGA Mark II reactor with the exception of samples vertically piled-up in a few mm and located in selected positions of CC and RB. In the remaining cases, e.g. when a large number or voluminous samples are simultaneously analyzed or the LS facility is used, monitors for k_0-NAA (or standards for relative-NAA) should surround the samples to receive the same flux. As an alternative, the effect of neutron flux parameters variations can be corrected taking into account the actual irradiation position of samples and monitors and using model functions calculated with previous data.

It is worth to note that the fast flux measured in LS was less than one twentieth of the fast flux measured in CC although the f at the bottom was (unexpectedly) close to the value measured in CC and RB. Since both the Hogdahl and the Westcott conventions do not consider the fast flux region, best results are obtained with k_0-NAA when the fast flux is negligible with respect to the thermal and epithermal fluxes. Moreover, threshold reactions produce interfering radionuclides that should be corrected both in relative- and k_0-NAA.

The knowledge of the regular trends observed in the TRIGA Mark II reactor of Pavia is useful to properly place samples, monitors and standards in order to limit the effect of gradients. In this context, the measurement of flux parameters should be repeated at fixed intervals or in case of rearrangement of the reactor core to check the time stability of the values.

6. Acknowledgment

Declarations of interest: none.

This research did not receive any specific grant from funding agencies in the

public, commercial, or not-for-profit sectors.

The authors would like to acknowledge Fausto Marchetti for direction of reactor operations, Fabio Zelaschi for sharing results of preliminary measurements, Barbara Smilgys for valuable discussion concerning the reactor configuration and, last but not least, Michele Prata, Giovanni Magrotti and the remaining LENA staff for the continuous all-around support.

AppendixA.

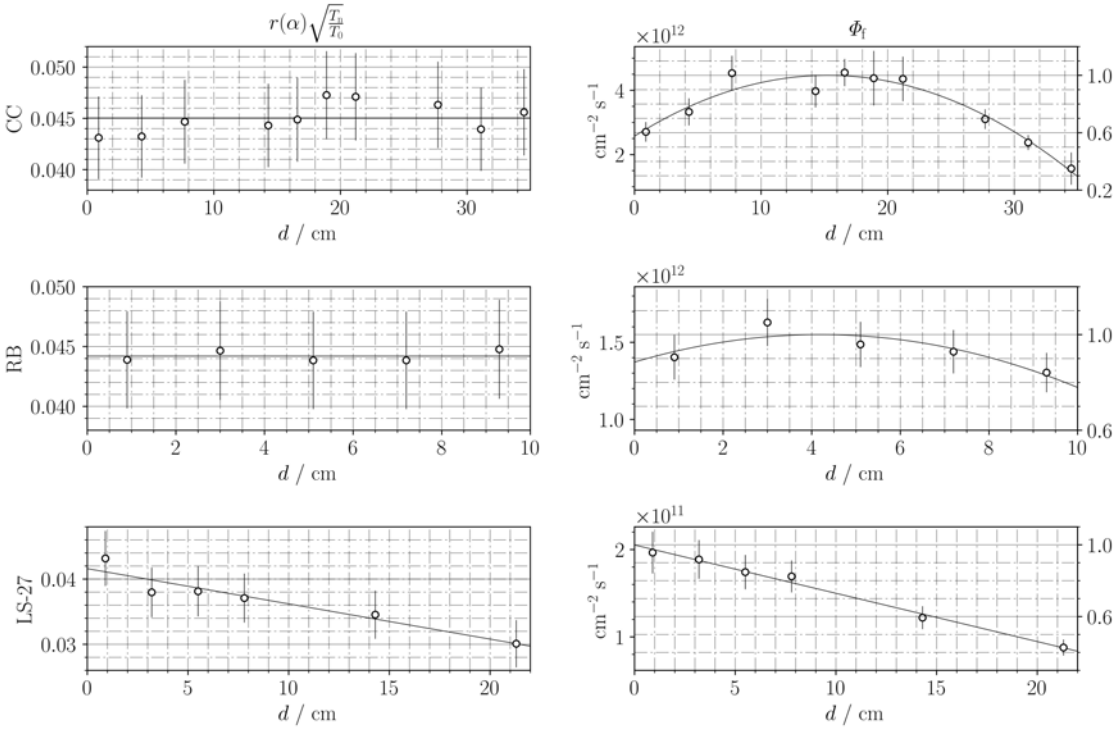

Figure A.1: The $r(\alpha)\sqrt{\frac{T_n}{T_0}}$ and Φ_f values measured in CC, RB and LS-27. Expanded uncertainties are reported with coverage factor $k = 2$. The solid lines display the averages, parabola or straight lines fitting the data.

References

[1] P. Bode, M. Blaauw, I. Obrusnik, Variation of neutron flux and related parameters in an irradiation container, in use with k_0-based Neutron Activation Analysis, J Radioanal Nucl Chem 157 (1992) 301–312. doi:10.1007/BF02047445.

[2] R. Jacimovic, P. Rogan, A. Trkov, Measurement and calculations of the neutron spectrum in different irradiation channels of the TRIGA Mark II reactor, Slovenia (2007).

[3] M. Di Luzio, M. Oddone, M. Prata, A. Salvini, G. D'Agostino, A preliminary test for the application of the k_0-standardization method of neutron activation analysis at the radiochemistry and spectroscopy laboratory of the Istituto Nazionale di Ricerca Metrologica, J Radioanal Nucl Chem 315 (2018) 723–729. doi:10.1007/s10967-017-5694-z.

[4] M. Di Luzio, M. Oddone, M. Prata, D. Alloni, G. D'Agostino, Measurement of the neutron flux parameters f and α at the pavia TRIGA Mark II reactor, J Radioanal Nucl Chem 312 (2017) 75–80. doi:10.1007/s10967-017-5191-4.

[5] F. De Corte, K. Sordo-El Hammami, L. Moens, A. Simonits, A. De Wispelaere, J. Hoste, The accuracy and precision of the experimental α-determination in the $1/E^{1+\alpha}$ epithermal reactor-neutron spectrum, J Radioanal Nucl Chem 62 (1981) 209–255. doi:10.1007/BF02517354.

[6] F. De Corte, The k_0-standardization method, 1987.

[7] F. De Corte, F. Bellemans, P. De Neve, A. Simonits, The use of a modified Westcott-formalism in the k_0-standardization of NAA: The state of affairs, J Radioanal Nucl Chem 179 (1994) 93–103. doi:10.1007/BF02037929.

[8] J. op de Beeck, Critical evaluation of the effective resonance energy concept and the epithermal neutron spectrum shape-factor α for reac-

tor NAA purposes, J Radioanal Nucl Chem 89 (1985) 169–190. doi:10.1007/BF02070214.

[9] N. E. Holden, Temperature dependence of the Westcott g-factor for neutron reactions in activation analysis, Pure Appl Chem 71 (1999) 2309–2315. doi:10.1351/pac199971122303.

[10] F. De Corte, A. Simonits, F. Bellemans, P. C. Freitas, S. Jovanovic, B. Smodis, G. Erdtmann, H. Petri, A. De Wispeleare, Recent advances in the k_0-standardization of neutron activation analysis: Extensions, applications, prospects, J Radioanal Nucl Chem 169 (1993) 125–158. doi:10.1007/BF02046790.

[11] R. van Sluijs, A. Stopic, R. Jacimovic, Evaluation of Westcott $g(T_n)$-factors used in k_0-NAA for non-$1/v$ (n,γ) reactions, J Radioanal Nucl Chem 306 (2015) 579–587. doi:10.1007/s10967-015-4134-1.

[12] M. Prata, D. Alloni, P. De Felice, M. Palomba, A. Pietropaolo, M. Pillon, L. Quintieri, A. Santagata, P. Valente, Italian neutron sources, Eur Phys J Plus 129 (2014) –. doi:10.1140/epjp/i2014-14255-3.

[13] L. Gacnik, K. Ambrozic, S. Rupnik, V. Radulovic, R. Jacimovic, Effect of control rod insertion on the TRIGA neutron spectrum and the determination of elemental concentrations with k_0-NAA, J Radioanal Nucl Chem 315 (2018) 711–721. doi:10.1007/s10967-018-5701-z.

[14] k_0 database.
URL http://www.kayzero.com/k0naa/k0naaorg/Nuclear_Data_SC/Entries/2016/1/11_New_k0-data_Library_2015.html

[15] M. Kostal, M. Schulc, V. Rypar, E. Losa, N. Burianova, J. Simon, M. Marecek, J. Uhlir, Validation of zirconium isotopes (n,γ) and (n,2n) cross sections in a comprehensive LR-0 reactor operative perameters set, Appl Radiat Isot 128 (2017) 92–100. doi:10.1016/j.apradiso.2017.06.023.

[16] J. Mejia, T. B. Coplen, M. Berglund, W. A. Brand, P. De Bievre, M. Groning, N. E. Holden, J. Irrgeher, R. D. Loss, T. Walczyk, T. Prohaska, Atomic weights of the elements 2013, Pure Appl Chem 88 (2016) 265–291. doi:10.1515/pac-2015-0305.

[17] H. Xiaolong, K. Mengxiao, Nuclear data sheets for A=198, Nucl Data Sheets 133 (2016) 221–416. doi:10.1016/j.nds.2016.02.002.

[18] P. Mohr, D. B. Newell, B. N. Taylor, CODATA recommended values of the fundamental physical constants: 2014, J Phys Chem Ref Data 45 (2016) 1–74. doi:10.1063/1.4954402.

[19] J. H. Hubbell, Photon mass attenuation and energy absorption coefficients from 1 keV to 20 MeV, J Appl Radiat Isotopes 33 (1982) 1269–1290. doi:10.1016/0020-708X(82)90248-4.

[20] A. Borio di Tigliole, A. Cammi, D. Chiesa, M. Clemenza, S. Manera, M. Nastasi, L. Pattavina, R. Ponciroli, S. Pozzi, M. Prata, E. Previtali, A. Salvini, M. Sisti, TRIGA reactor absolute neutron flux measurement using activated isotopes, Prog Nucl Energy 70 (2014) 249–255. doi:10.1016/j.apradiso.2017.06.023.